Supplement of Atmos. Chem. Phys., 22, 7713–7726, 2022
https://doi.org/10.5194/acp-22-7713-2022-supplement

Atmospheric Chemistry and Physics
Open Access

Supplement of

Strong light scattering of highly oxygenated organic aerosols impacts significantly on visibility degradation

Li Liu et al.

Correspondence to: Ye Kuang (kuangye@jnu.edu.cn)

Table of contents

1. Site information

The observation site locates in Haizhu wetland park, which is surrounded by roads, business, and residential districts, however, at least ~1 km away from the observation site.

Figure S1. Site environments and the container (green one).

2.Q-ACSM analysis

In this study, organic aerosol (OA) spectra measured by the Q-ACSM were deconvolved into OA factors using an improved source apportionment technique called Multilinear Engine (ME-2) which is an upgrade of widely used Positive Matrix Factorization (PMF) technique and runs on a IGOR-based interface [1]. Different with traditional PMF, ME-2 offers a coefficient called a-value to constrain the spectra

variation extent of OA factor with given priori mass spectra [1, 2]. The unconstrained runs with PMF technique were firstly performed with possible factor number of 2-8. It was found that four factors solution splits clearly OA factors, with solutions of 3 or 5 factors show less or over split features. Results for factor number determination were shown in Fig.S2-5. For example, three factors solution does not split two major primary OA factors of cooking-like OA (COA) and hydrocarbon-like OA (HOA) in urban area, and five factor solutions over split the oxygenated organic aerosol, thus four factors solution was finally determined as the best. However, previous studies demonstrate that PMF solution sometimes failed in clean separating OA factors [1, 2]. Similar case was also found in the unconstrained solution as shown in Fig.S4 that the factor 1 showed obvious cooking-like primary OA (COA) features (for example high correlations with m/z 55, and obvious noon peak), however showing higher oxidation feature than previously reported results of COA with exceptionally high m/z 44 fraction [2], thus the solution has defects. The a-value approach of ME-2 techniques provides additional constrains on factors through introducing user defined external factor mass spectra profile, however a priori mass spectra of COA for Q-ACSM measurements in Guangzhou urban area is lacking. Chinese spring festival (area shaded with pink color in Figure 1 of the manuscript) was during the observation period and stay home policy was recommended by Chinese government due to the COVID-19 epidemic, thus very small traffic flow however might even higher cooking activities than usual due to the festival celebration. Results of Guo, et al. (2020)[2] demonstrate that COA usual contribute even slightly higher than HOA (Hydrocarbon-like OA), suggesting that the dominant contribution of COA to primary OA during the special "spring festival and COVID epidemic stay home" period, thus provide us a unique opportunity to identify spectra profile that most close to realistic COA spectra. The unconstrained PMF technique performed specific to the spring festival period from 11th to 25th February 2021, and five factor solution with most prominent COA features was determined **(**Fig.S6-7) although might over spilt the oxygenated OA. The factor with obvious COA feature was chosen as the used defined external spectra in ME-2 of four factor solutions with a values range from 0.1 to 0.5.

The ME-2 solution with a value of 0.2 was adopted based on correlation coefficients with external tracers, and solutions of a values ranging from 0.1 to 0.3 as well as their correlation coefficients with external tracers are shown in Fig.S8-10. Compared with results of the unconstrainted PMF, correlations of COA factor with m/z 55 has improved substantially (R^2 increased from 0.49 to 0.77), and the determined COA factor has much better COA features and lower O/C [3]. Note the O/C value of factors were estimated using the empirical relationship between f_{44} and O/C proposed by Aiken, et al. (2008)[4].

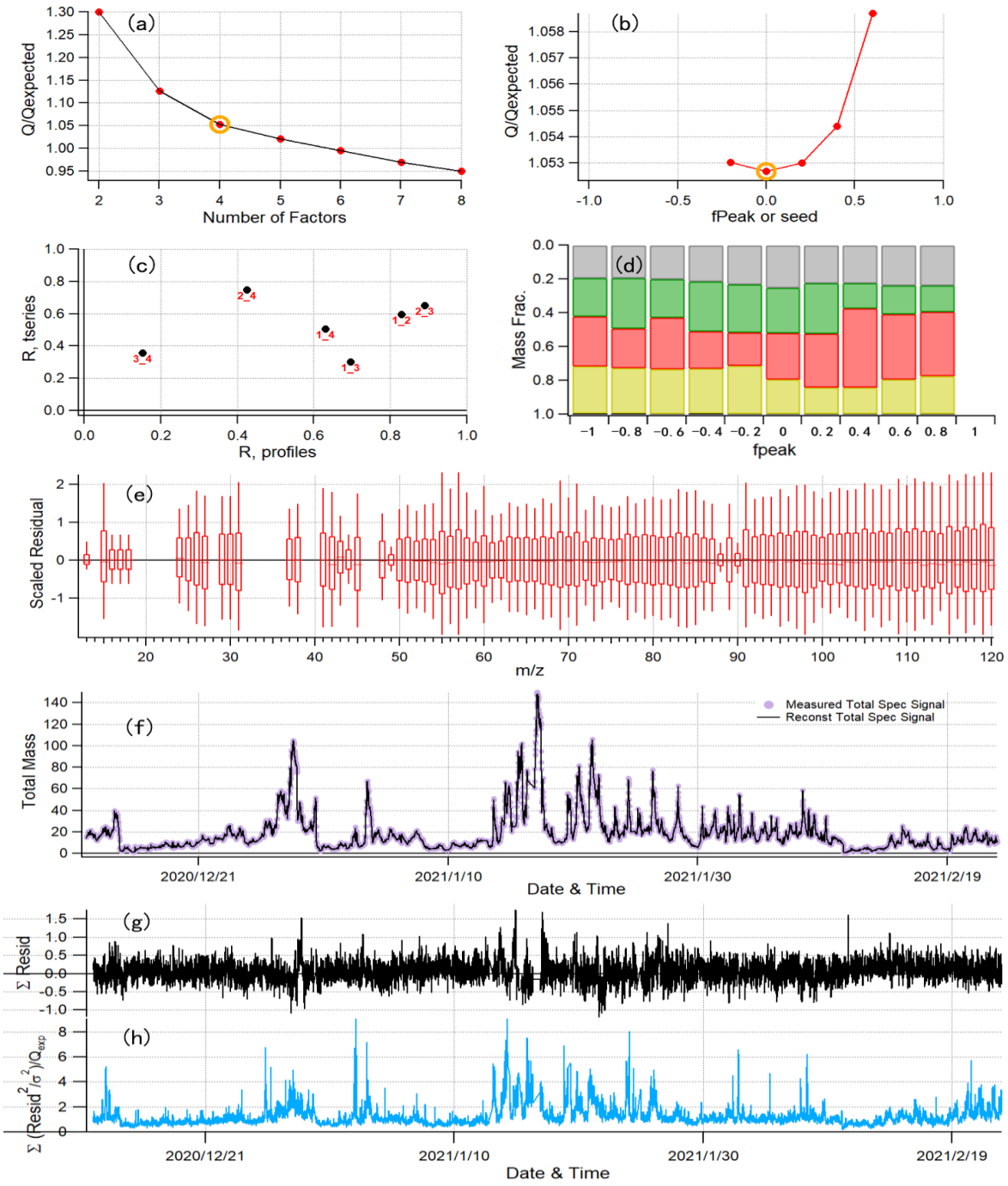

127 **Figure S2**. Diagnostic plots of the 4-factor solution in the unconstrained PMF.

128
129
130
131
132
133
134

PMF results

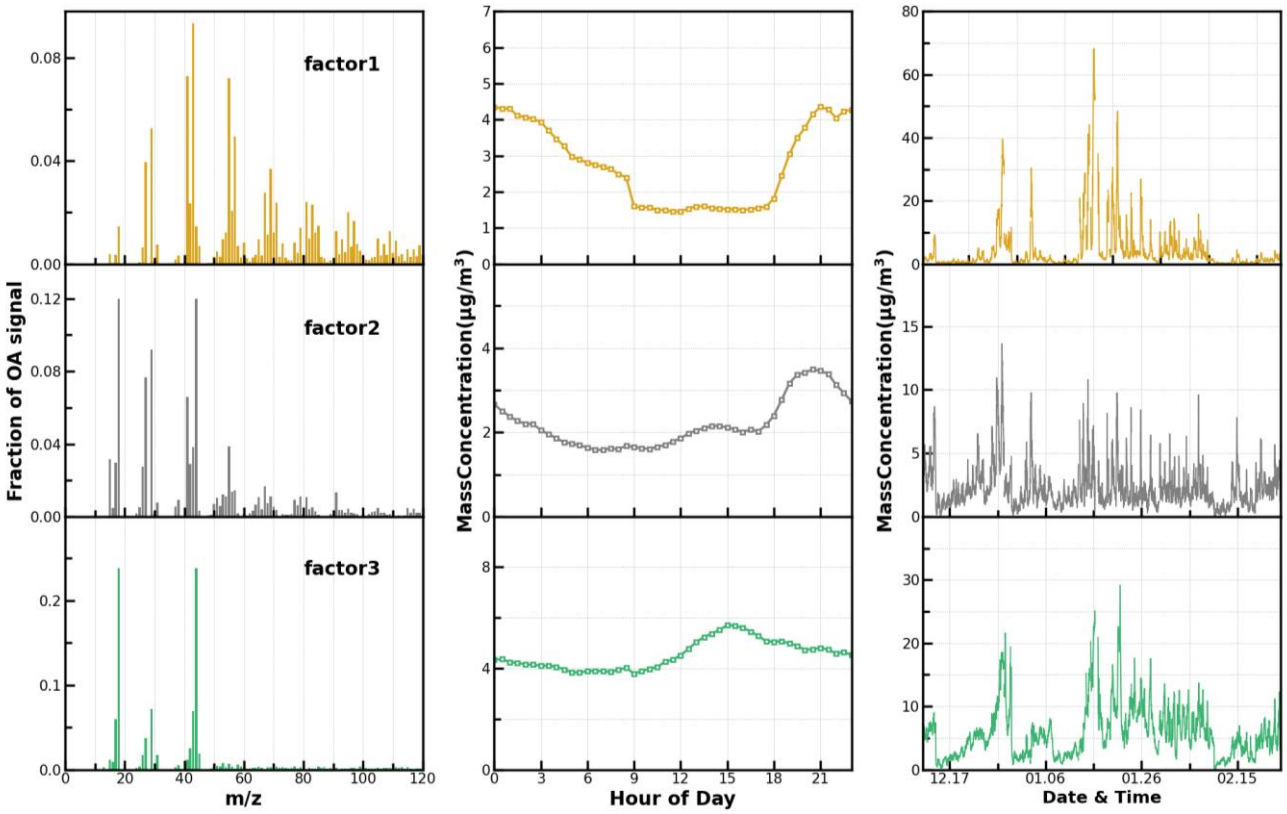

Figure S3. Mass spectra, diurnal variations and time series of 3-factor solution from unconstrained PMF.

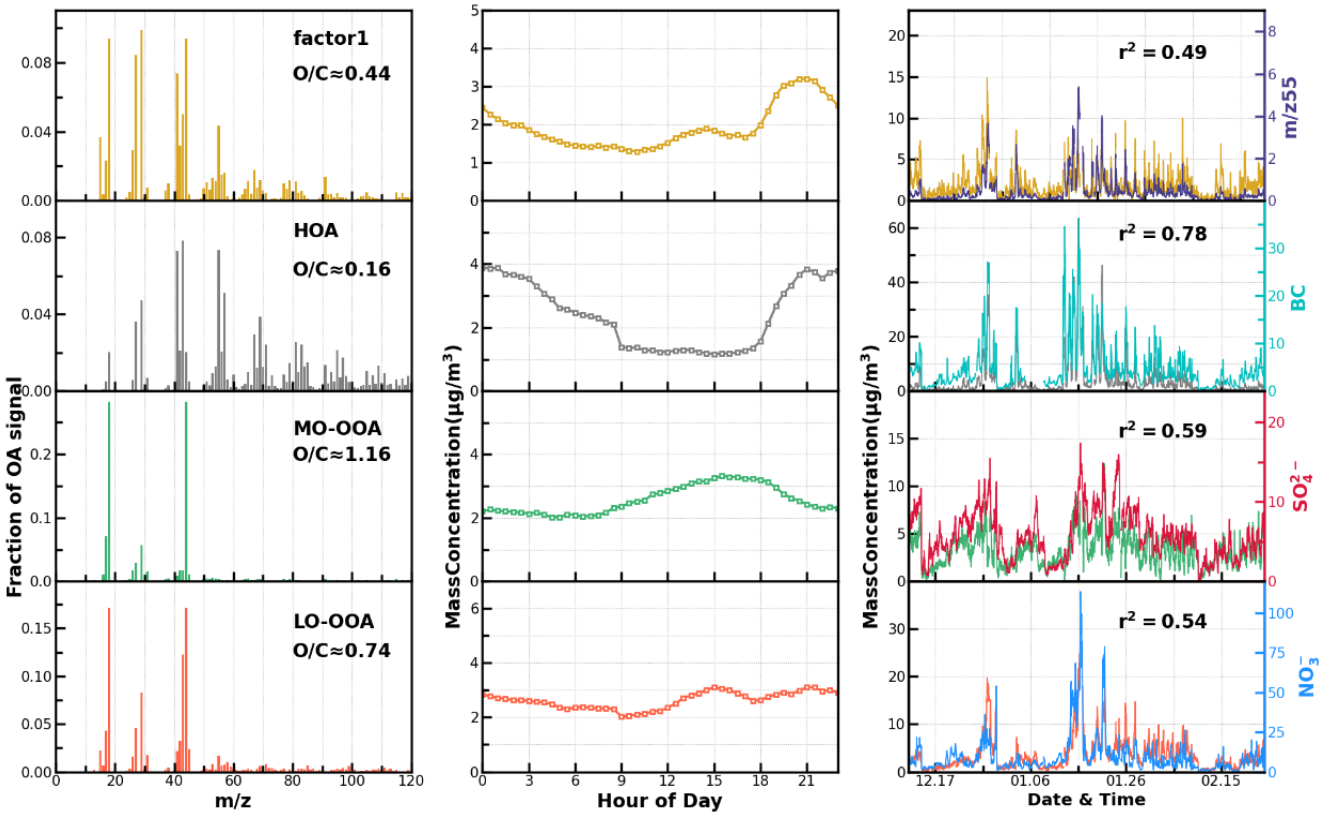

156 **Figure S4.** Mass spectra, diurnal variations, and time series of 4-factor solution from
157 unconstrained PMF.

158
159
160
161
162
163
164
165
166
167
168
169
170
171
172
173
174
175

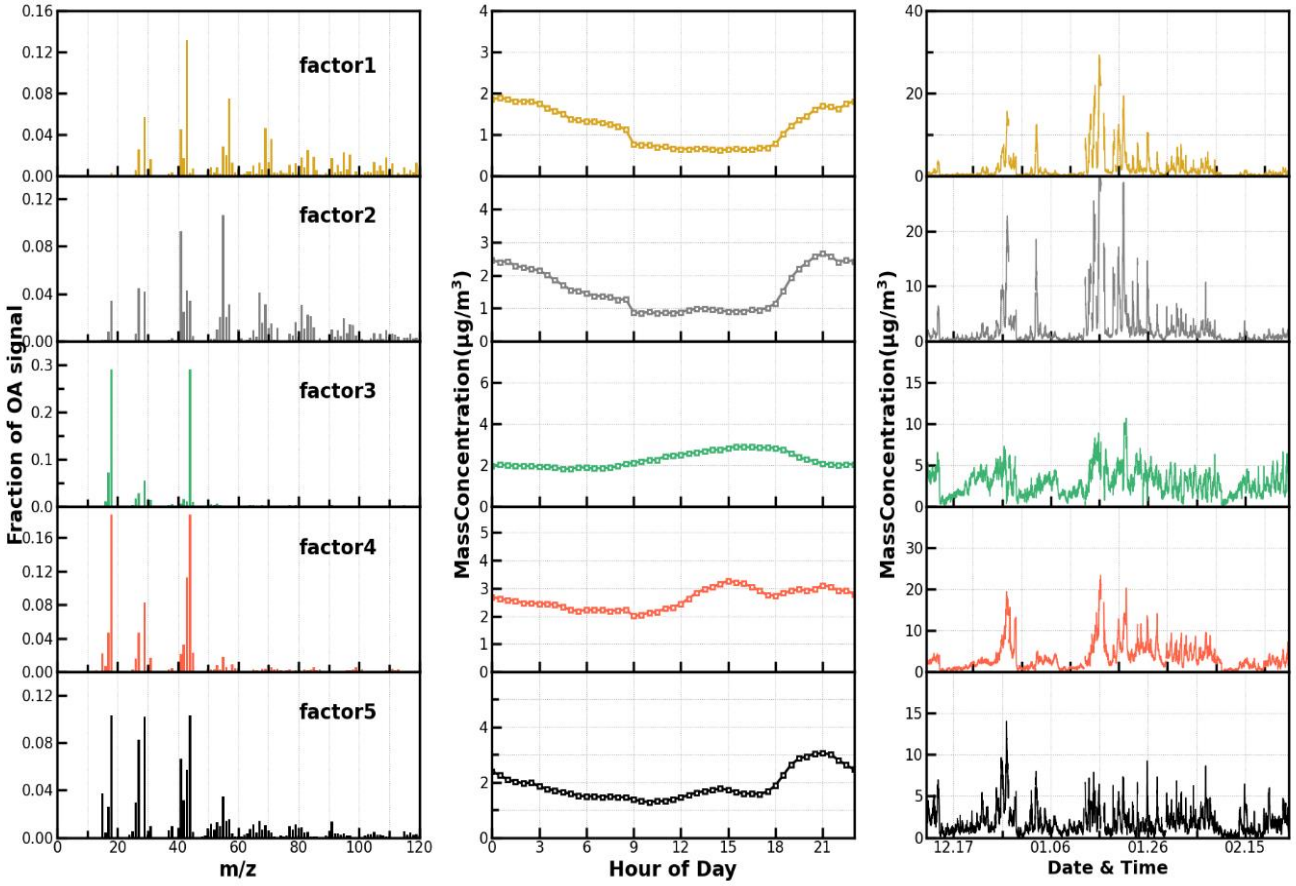

Figure S5. Mass spectra, diurnal variations, and time series of 5-factor solution from unconstrained PMF.

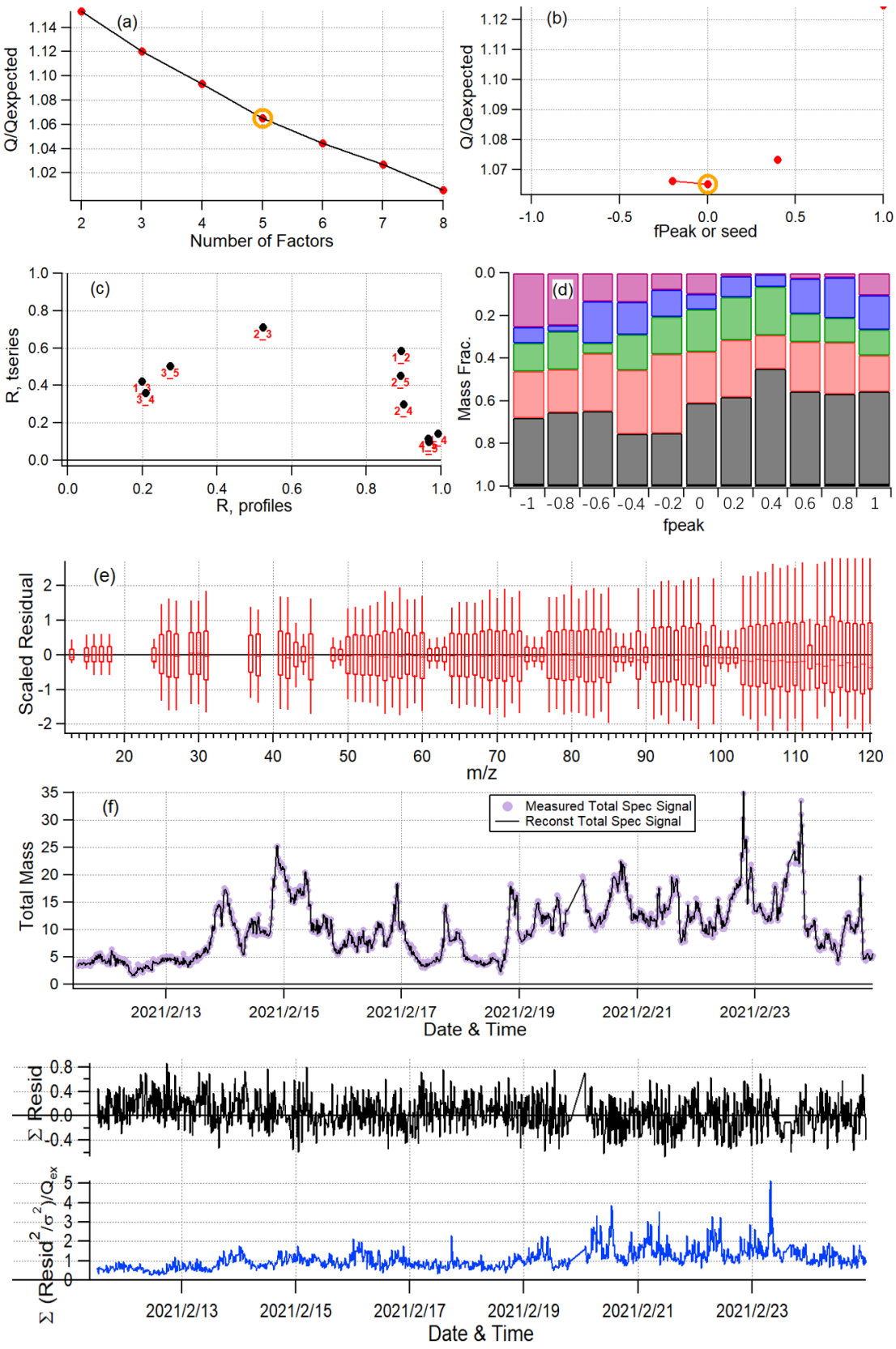

195 **Figure S6**. Diagnostic plots of the 5-factor solution in the unconstrained PMF during
196 the spring festival period from 11th to 25th February 2021.

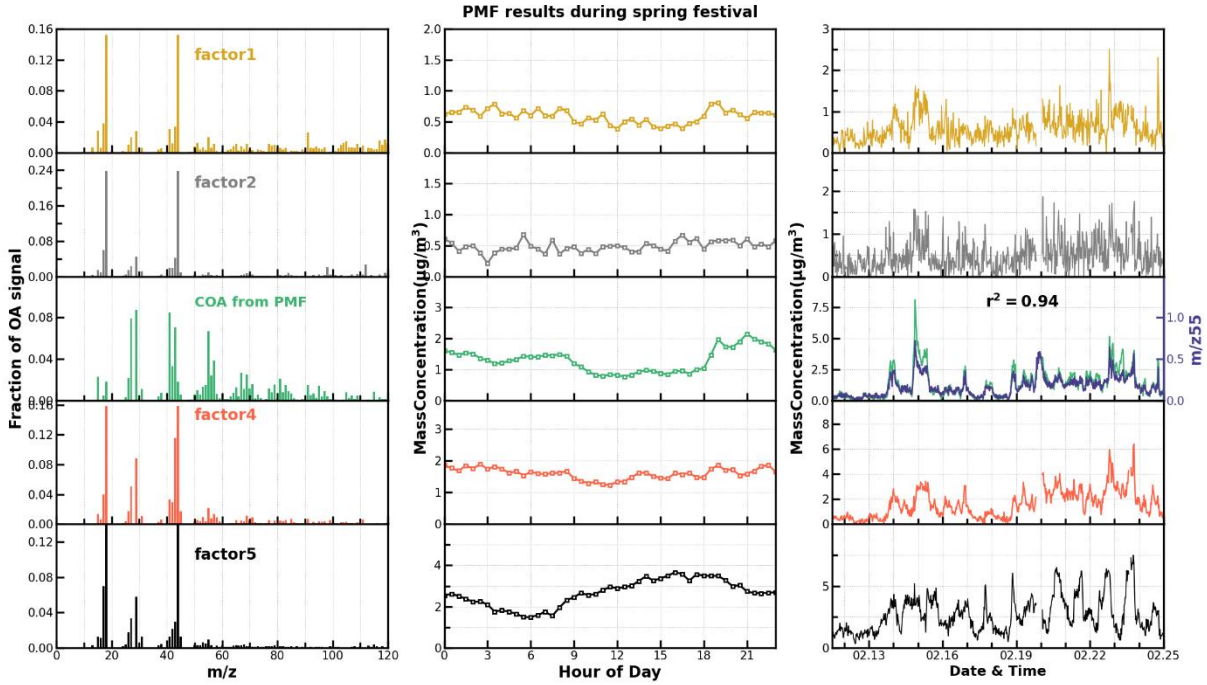

Figure S7. Mass spectra, diurnal variations, and time series of 5-factor solution from unconstrained PMF during the spring festival period from 11th to 25th February 2021.

ME-2 results

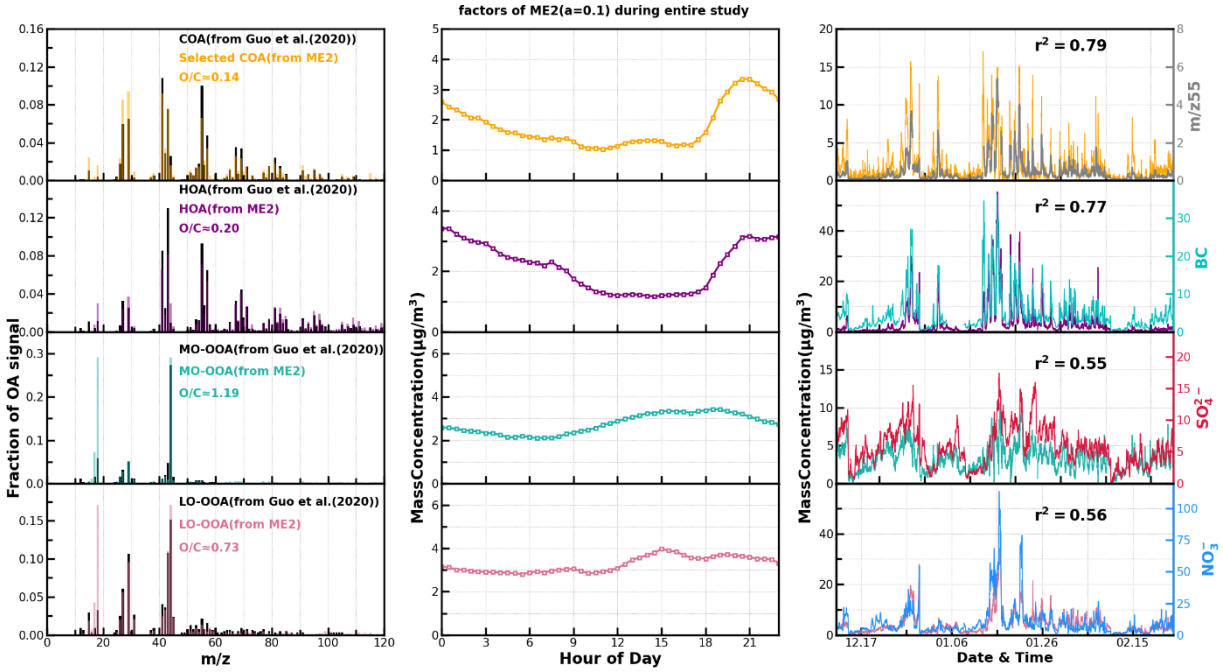

Figure S8. Mass spectra, diurnal variations, and time series of ME-2(a-value=0.1) under the 4-factor solution.

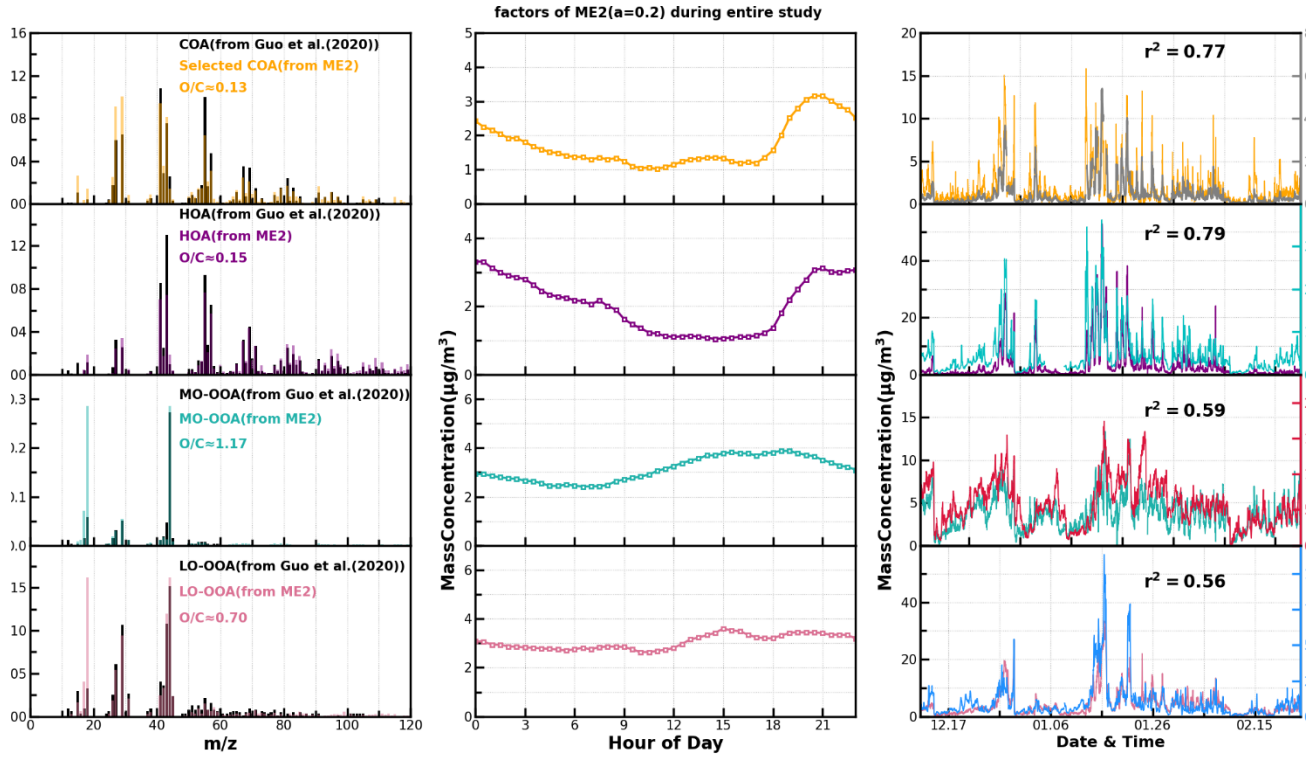

Figure S9. Mass spectra, diurnal variations, and time series of ME-2(a-value=0.2) under the 4-factor solution.

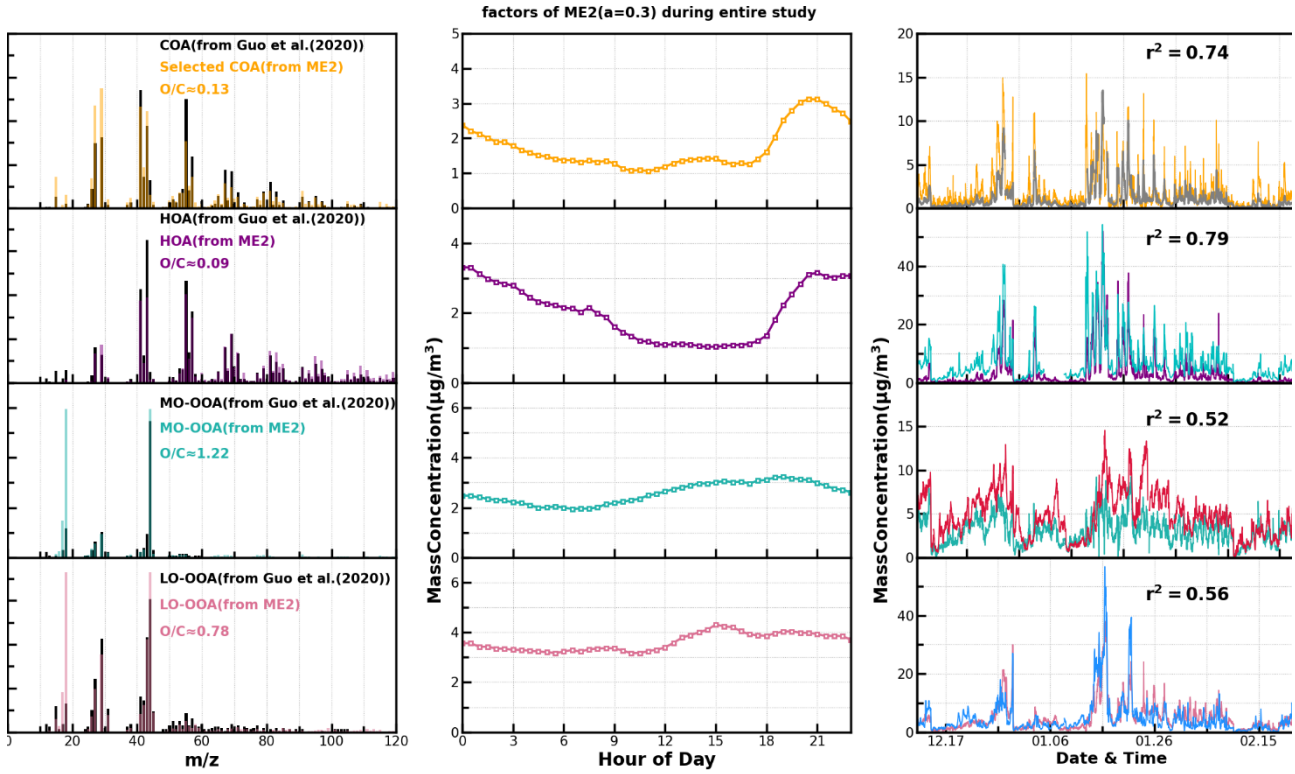

Figure S10. Mass spectra, diurnal variations, and time series of ME-2(a-value=0.3) under the 4-factor solution.

3. Discussions on traditional multilinear regression model

In this study, we tried to perform the traditional multiple linear regression analysis with HOA, COA, LOOA, MOOA, AS (ammonium sulfate), AN (ammonium nitrate) and BC as input variables and aerosol scattering coefficients as target variable. Note that ammonium nitrate (AN) and ammonium sulfate (AS) were determined as the dominant form of ammonium, and paired spot of ammonium bisulfate was treated as AS in the multiple linear regression model due to their similarity in scattering abilities. Negative MSE_{LOOA} were obtained if MSE values were not constrained, and MSEs of some aerosol components deviated significantly from previously reported ranges. If MSEs of aerosol components were constrained as positive, then an MSE_{LOOA} of zero

would be obtained. These results demonstrate that the multiple regression model failed in retrieving aerosol MSE, and two reasons might be responsible for this failure. The first one is mathematically fundamental, the application of multiple linear regression model perform best with independent input variables, however, the square of correlation coefficients (R^2) between several variables were higher than 0.5 for datasets of this study (Table.S2). For example, the square of correlation coefficients between HOA and LOOA, between LOOA and AN, and between HOA and BC are 0.6, 0.54 and 0.78 respectively. The second reason is associated with the observations that aerosol scattering of entire aerosol populations of $PM_{2.5}$ were measured however part of the aerosol mass such as PM_1 dust were not identified by the mass spectrometer [5, 6] and the contribution of unidentified part might varies substantially [7]. In addition, aerosol scattering coefficients of $PM_{2.5}$ were measured whereas mass concentrations of PM_1 were quantified.

Table S1. Square of correlation coefficients between aerosol components

	COA	LOOA	MOOA	BC	AS	AN
HOA	**0.37**	**0.6**	**0.11**	**0.79**	**0.16**	**0.39**
COA		**0.42**	**0.1**	**0.43**	**0.15**	**0.17**
LOOA			**0.37**	**0.57**	**0.43**	**0.54**
MOOA				**0.12**	**0.59**	**0.49**
BC					**0.22**	**0.33**
AS						**0.28**

Table S2. Square of correlation coefficients between changes of aerosol components for identified cases

	△COA	△LOOA	△MOOA	△BC	△AS	△AN
△HOA	**0.34**	**0.44**	**0.43**	**0.88**	**0.01**	**0.02**
△COA		**0.34**	**0.56**	**0.29**	**0.05**	**0.07**
△LOOA			**0.38**	**0.5**	**0.00**	**0.03**
△MOOA				**0.4**	**0.12**	**0.07**
△BC					**0.02**	**0.01**
△AS						**0.39**

4. Visibility contributions estimation

Based on the Koschmieder theory, atmospheric visibility is determined by atmospheric extinction coefficient σ_{ex} [8]:

$$\text{Visibility} = \frac{K}{\sigma_{ex}} \quad . \qquad \text{Eq. S1}$$

Where K is the Koschmieder constant, and a value of 3.0 is usually used for Asian people and thus also visibility meter [9]. The σ_{ex} is the total atmospheric light extinction coefficient at 550 nm caused by aerosols and air molecules and can be calculated through the sum of its scattering and absorption components:

$$\sigma_{ex} = \sigma_{sp} + \sigma_{abs} + \sigma_{air} + \sigma_{NO_2}, \qquad \text{Eq. S2}$$

where σ_{sp} and σ_{abs} are the aerosol scattering and absorption coefficients, σ_{air} is the Rayleigh scattering by air molecules and σ_{NO_2} the absorption by NO_2 molecules. Rayleigh scattering of air molecules at 550 nm under standard atmospheric pressure is about 13 Mm^{-1} [10]. The NO_2 absorption at 550 nm is calculated using $\sigma_{NO_2} = 0.33 \cdot [NO_2]$,where $[NO_2]$ represents the NO_2 volume mixing ratio in units of ppb, and unit of calculated σ_{NO_2} is Mm^{-1}. Aerosol absorptions at 520 and 590 nm measured by the AE33 aethalometer were used to calculate aerosol absorptions (σ_{abs}) at 550 nm through absorption Ångström law.

As to the aerosol scattering σ_{sp} at 550 nm, it can be calculated as based on analysis of Xu, et al. (2020)[9]:

$$\sigma_p = \sigma_{sp,fine} + \sigma_{sp,coarse} = \sigma_{sp,PM_{2.5}}(RH) + 0.036 \cdot \sigma_{sp,PM_{2.5}(dry)} \quad \text{Eq. S3}$$

Where direct measurements of $\sigma_{sp,PM_{2.5}(dry)}$ at 525 nm were converted to $\sigma_{sp,PM_{2.5}(dry)}$ at 550 nm using measured between scattering Ångström exponent by the nephelometer. The $\sigma_{sp,PM_{2.5}}(RH)$ values at 525 nm were firstly calculated as the summation of aerosol scattering coefficients of MOOA, LOOA, HOA, COA, BC, AN and AS under ambient RH conditions by considering MSE values derived at 525 nm and aerosol hygroscopicity:

$$\sigma_{sp,PM_{2.5}}(RH) = \sigma_{sp,MOOA,PM_{2.5}}(RH + \sigma_{sp,LOOA,PM_{2.5}}(RH) + \sigma_{sp,HOA,PM_{2.5}}(RH) +$$

$$\sigma_{sp,COA,PM_{2.5}}(RH) + \sigma_{sp,BC,PM_{2.5}}(RH) + \sigma_{sp,AS,PM_{2.5}}(RH) + \sigma_{sp,AN,PM_{2.5}}(RH) \quad \text{Eq. S4}$$

COA, BC, HOA are hydrophobic with hygroscopic parameter κ of zero. Thus, their scattering didn't change with ambient RH and are same with their values in dry state.

In addition, as discussed in Sect.4.2 of the manuscript, most HOA, COA and BC mass reside in PM1. Thus, $\sigma_{sp,HOA,PM_{2.5}}(RH) = [HOA]_{PM1} \times MSE_{HOA,PM1}(dry)$, $\sigma_{sp,COA,PM_{2.5}}(RH) = [COA]_{PM1} \times MSE_{COA,PM1}(dry)$, and $\sigma_{sp,BC,PM_{2.5}}(RH) = [BC]_{PM1} \times MSE_{BC,PM1}(dry)$ where [X] represents mass concentrations of aerosol components [X]. For hydrophilic aerosol components, MOOA, LOOA, AS, and AN, their scattering under ambient RH conditions were calculated using $\sigma_{sp,MOOA,PM_{2.5}}(RH) = [MOOA]_{PM1} \times MSE^*_{MOOA} \times \kappa_{MOOA} \times R_{sca,MOOA}$, $\sigma_{sp,LOOA,PM_{2.5}}(RH) = [LOOA]_{PM1} \times MSE^*_{LOOA} \times \kappa_{LOOA} \times R_{sca,LOOA}$, $\sigma_{sp,AS,PM_{2.5}}(RH) = [AS]_{PM1} \times MSE^*_{AS} \times \kappa_{AS}(RH) \times R_{sca,AS}$, and $\sigma_{sp,AN,PM_{2.5}}(RH) = [AN]_{PM1} \times MSE^*_{AN} \times \kappa_{AN}(RH) \times R_{sca,AN}$. As discussed in Sect.4.4 of the manuscript, $R_{sca,LOOA}$ is 0.87, and 0.63 for $R_{sca,MOOA}$, $R_{sca,AS}$ and $R_{sca,AN}$. MSE^*_X defined as $MSE^*_X = \frac{\sigma_{sp,525}(PM_{2.5})}{[X](PM_1)}$ for aerosol components were retrieved and discussed in Sect.4.2 of the manuscript. $\sigma_{sp,X,PM_{2.5}}(RH)$ values at 550 nm of aerosol components X were then converted to 550 nm using measured scattering Ångström exponent. Contributions of aerosol components to visibility degradation were thus calculated as:

$$Contribution = \frac{\sigma_{sp,X,PM_{2.5}}(RH, 550\ nm)}{\sigma_{ex}(550\ nm)}$$

5. Other Figures

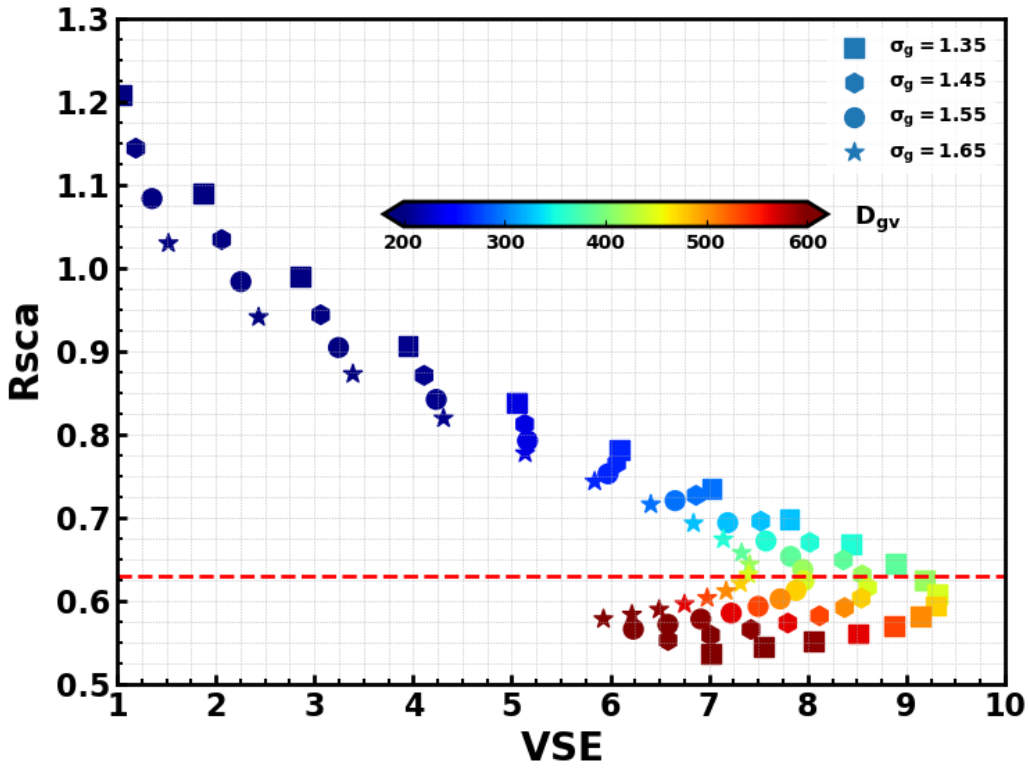

Figure S11. Simulated relationships between VSE_{PM1} and Rsca using Mie theory through varying volume geometric mean D_{gv} of lognormal size distributions from 100 to 700 nm under different standard deviation ($\boldsymbol{\sigma_g}$) conditions.

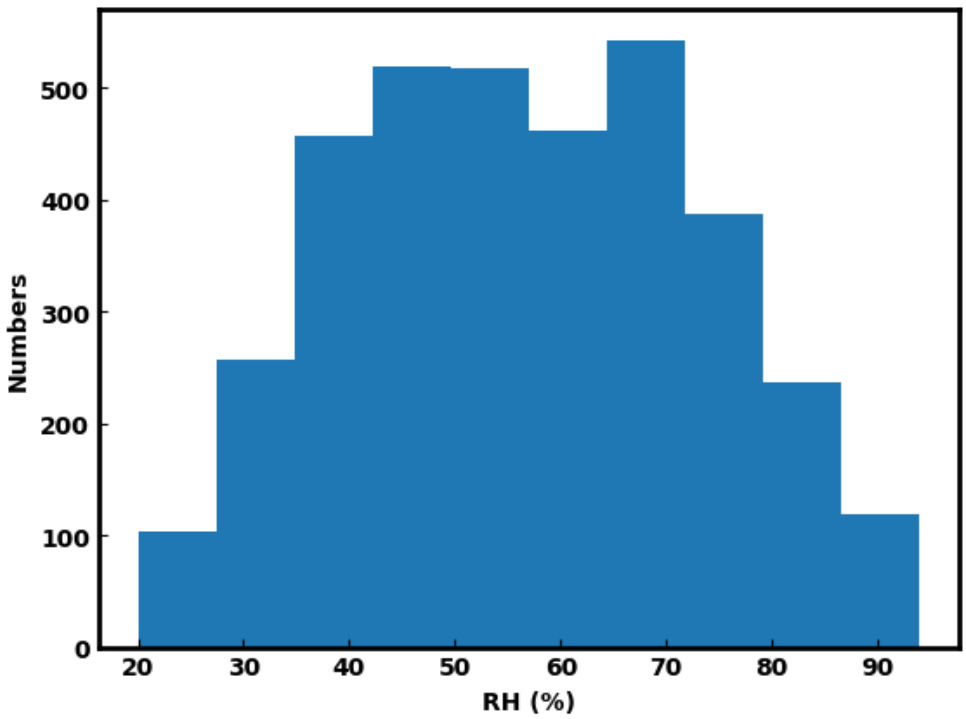

Figure S12. Histogram of ambient relative humidity (RH) during the observation period.

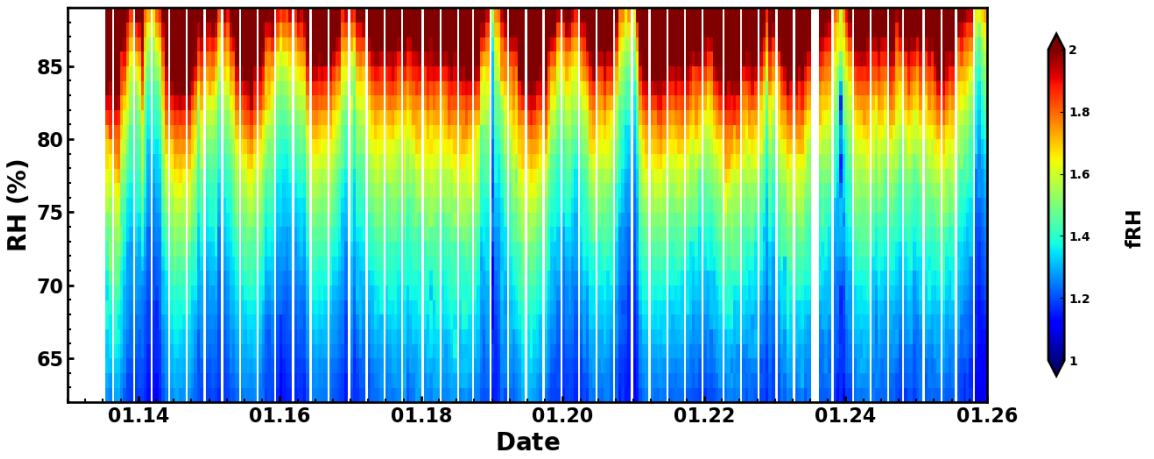

Figure S13. Aerosol light scattering enhancement measurements (fRH) at 525 nm from 13th to 26th February with RH range of 60-90%.

References

1. Canonaco, F.; Crippa, M.; Slowik, J. G.; Baltensperger, U.; Prévôt, A. S. H., SoFi, an IGOR-based interface for the efficient use of the generalized multilinear engine (ME-2) for the source apportionment: ME-2 application to aerosol mass spectrometer data. *Atmos. Meas. Tech.* **2013,** *6*, (12), 3649-3661.
2. Guo, J.; Zhou, S.; Cai, M.; Zhao, J.; Song, W.; Zhao, W.; Hu, W.; Sun, Y.; He, Y.; Yang, C.; Xu, X.; Zhang, Z.; Cheng, P.; Fan, Q.; Hang, J.; Fan, S.; Wang, X.; Wang, X., Characterization of submicron particles by time-of-flight aerosol chemical speciation monitor (ToF-ACSM) during wintertime: aerosol composition, sources, and chemical processes in Guangzhou, China. *Atmospheric Chemistry and Physics* **2020,** *20*, (12), 7595-7615.
3. Sun, Y. L.; Wang, Z. F.; Fu, P. Q.; Yang, T.; Jiang, Q.; Dong, H. B.; Li, J.; Jia, J. J., Aerosol composition, sources and processes during wintertime in Beijing, China. *Atmos. Chem. Phys.* **2013,** *13*, (9), 4577-4592.
4. Aiken, A. C.; DeCarlo, P. F.; Kroll, J. H.; Worsnop, D. R.; Huffman, J. A.; Docherty, K. S.; Ulbrich, I. M.; Mohr, C.; Kimmel, J. R.; Sueper, D.; Sun, Y.; Zhang, Q.; Trimborn, A.; Northway, M.; Ziemann, P. J.; Canagaratna, M. R.; Onasch, T. B.; Alfarra, M. R.; Prevot, A. S. H.; Dommen, J.; Duplissy, J.; Metzger, A.; Baltensperger, U.; Jimenez, J. L., O/C and OM/OC Ratios of Primary, Secondary, and Ambient Organic Aerosols with High-Resolution Time-of-Flight Aerosol Mass Spectrometry. *Environmental science & technology* **2008,** *42*, (12), 4478-4485.
5. Shao, L.; Li, W.; Yang, S.; Shi, Z.; Lü, S., Mineralogical characteristics of airborne particles collected in Beijing during a severe Asian dust storm period in spring 2002. *Science in China Series D: Earth Sciences $V 50* **2007**, (6), 953-959.
6. Ng, N. L.; Herndon, S. C.; Trimborn, A.; Canagaratna, M. R.; Croteau, P. L.; Onasch, T. B.; Sueper, D.; Worsnop, D. R.; Zhang, Q.; Sun, Y. L.; Jayne, J. T., An Aerosol Chemical Speciation Monitor (ACSM) for Routine Monitoring of the Composition and Mass Concentrations of Ambient Aerosol. *Aerosol Science and Technology* **2011,** *45*, (7), 780-794.
7. Kuang, Y.; He, Y.; Xu, W.; Zhao, P.; Cheng, Y.; Zhao, G.; Tao, J.; Ma, N.; Su, H.; Zhang, Y.; Sun, J.; Cheng, P.; Yang, W.; Zhang, S.; Wu, C.; Sun, Y.; Zhao, C., Distinct diurnal variation in organic aerosol hygroscopicity and its relationship with oxygenated organic aerosol. *Atmos. Chem. Phys.* **2020,** *20*, (2), 865-880.
8. Chen, J.; Zhao, C. S.; Ma, N.; Liu, P. F.; Göbel, T.; Hallbauer, E.; Deng, Z. Z.; Ran, L.; Xu, W. Y.; Liang, Z.; Liu, H. J.; Yan, P.; Zhou, X. J.; Wiedensohler, A., A parameterization of low visibilities for hazy days in the North China Plain. *Atmos. Chem. Phys.* **2012,** *12*, (11), 4935-4950.
9. Xu, W.; Kuang, Y.; Bian, Y.; Liu, L.; Li, F.; Wang, Y.; Xue, B.; Luo, B.; Huang, S.; Yuan, B.; Zhao, P.; Shao, M., Current Challenges in Visibility Improvement in Southern China. *Environmental Science*

484 *& Technology Letters* **2020**.
485 10. Liu, X.; Cheng, Y.; Zhang, Y.; Jung, J.; Sugimoto, N.; Chang, S.-Y.; Kim, Y. J.; Fan, S.; Zeng, L.,
486 Influences of relative humidity and particle chemical composition on aerosol scattering properties
487 during the 2006 PRD campaign. *Atmospheric Environment* **2008,** *42*, (7), 1525-1536.
488